DESIGN OF A FLEXURE-BASED RESONANT TRANSLATING MICROMIRROR

Premkumar Sivakumar
UCLA Mechanical and Aerospace Engineering
Los Angeles, CA, U.S.A.

ABSTRACT

This report proposes a design of a flexure-based translating micromirror operated at its resonant frequency driven by repulsive electrostatic force. The device is meant to modulate the phase of light reflected off of its surface for a variety of high-impact precision applications such as adaptive optics. Besides achieving single translation DOF orthogonal to the reflective surface, other design considerations include the minimization of parasitic errors, minimization of over-constrained and under-constrained topology and fabrication feasibility. A single-degree of freedom model is used based on the FACT approach for compliant mechanism design to guide the design process. Behavior of the design is analyzed through calculations of the resonant frequencies and their corresponding mode shapes in MATLAB, and validated using FEA based modal analysis in ANSYS and SolidWorks. The design is to be fabricated using a CMOS compatible SOI process.

INTRODUCTION

Micromirrors are among the oldest kind of MEMS solutions which were investigated. Among the different applications which drove the earlier interest in this type of technology, we can find confocal microscopy, laser printing, bar code reading, switching and interconnection in optical communications. The current applications of micromirrors are found in optical communication, switching, digital projection, adaptive optics, lithography, medical applications, optical filters, spectrometers, interferometers, sensorics, smart glass in buildings, personalized light steering heat management, optical shutters, car headlights, displays, ion batteries, gas storage, energy harvesting, solar cell back reflectors, compact waveguides and nano-cavity devices.

Vertical translation micromirrors in particular are key components in Micro-Opto-Electro-Mechanical Systems (MOEMS) and are used in adaptive optics to improve the performance of imaging systems by correcting the wave front aberration induced by atmospheric turbulence or imperfections in system components. A vertically translating micromirror can be used to modulate the phase of light reflected off of its surface for a variety of high-impact precision application like adaptive optics. Such mirrors are often driven to operate at their resonant frequencies.

Resonant operation is a mode of operation in which the micromirror is driven at the frequency of its natural vibration mode. In this condition, the mechanical structure itself responds with an amplified movement. Typically, a resonant operation is used to achieve large out-of-plane amplitudes. Operating at the resonant frequencies minimizes the system's required actuation energy and simplifies the mirror's control such that no sensors or closed-loop control circuitry is needed to achieve the desired speed.

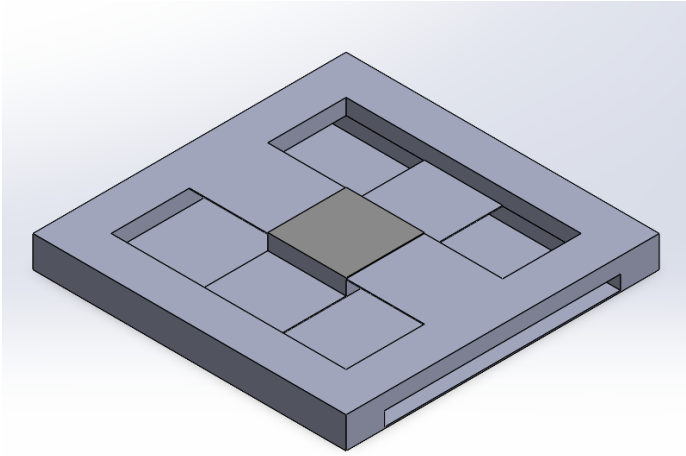

FIGURE 1: DESIGN OF PARALLEL FLEXURE SYSTEM FOR A RESONANT TRANSLATING MICROMIRROR

The following sections give further explanation of the behavior of such a device and a description of an initial attempt to create such a device. Afterward, a new design is presented and analyzed via a single degree of freedom model and a finite element model.

BACKGROUND

The objective of this project is to design a flexure system for a resonant translating micromirror. Prior works have investigated high-speed micromirrors with different flexure systems, topological designs, modes of operation, actuation methods and fabrication techniques. Siyuan He et al [7][8] developed a novel translation micromirror for adaptive optics using a repulsive electrostatic force. Repulsive electrostatic force actuation overcomes the limitations associated with conventional translation micromirrors and its stroke is not limited by the initial gap distance between the mirror plate and the substrate and therefore is able to achieve a much larger vertical stroke to

modulate lights over a wider spectrum than that achieved by conventional translation micromirrors. The novel translation micromirror has no stiction problem and is highly compatible with mature surface micromachining technology. This design achieved a vertical stroke of 1.75 μm using a driving voltage of 50 volts which is three times the stroke of conventional MUMPS translation micromirrors.

Sandner et al [16] developed a translatory MOEMS actuator for fast optical path length modulation in a miniaturized Fourier transform infrared spectrometer. The device is driven electrostatically resonant using in-plane comb drives and is manufactured in a CMOS compatible silicon-on-insulator process. Two designs were proposed, the first of which used bending springs and achieved a 200 μm stroke with low voltages (<40 V) at an ambient pressure below 500 Pa. Consequently, this yields a spectral resolution of 25 cm^{-1} and an acquisition time of 200 μs per spectrum. The second design used a larger aperture mirror and two pantograph suspensions enabling higher amplitude stroke of up to 500 μm, improved spectral resolution of 10 cm^{-1} and signal-to-noise ratio of >1000:1.

A later work by the same author [17] involved four pantograph suspensions in fourfold rotationally symmetric configuration to realize a larger stroke of the mirror plate of up to 1.2 mm without any parasitic tilting of the fast-oscillating mirror. Up to 1 mm stroke was measured in vacuum of 30 Pa and 50 V driving voltage.

Other works involve other DOFs in addition to translation or just torsional DOF. F-Y. Lee et al [6] developed a micromirror tunable resonant frequency. The device uses comb-drive operated at resonance due to the limited force/energy density of electrostatic actuators. Errors in microfabrication processes often cause natural frequencies to offset from the design value. This issue is resolved by a frequency-tunable micromirror. The shifting of the resonant frequency is achieved by adjusting the axial stress of the micromirror's torsion hinge via integrated chevron thermomechanical actuators.

R. Farrugia et al [15] presented a structural design optimization scheme for a one directional resonant micromirror intended for laser projection with XGA optical resolution. The minimization of dynamic deformation is considered as one of the partial objectives of this work together with other micromirror performance and reliability characteristics. This design process demonstrates the technical feasibility of including features, such as a gimbal structure, that improve the dynamic mirror flatness without compromising on the target scanning frequency, mode separation and maximum shear stress.

Besides the resonant translation micromirrors, prior work has been done in developing quasi-static micromirrors as well. Quasi-static operation is a mode of operation where the micromirror can be driven with an arbitrary waveform. Typical quasi-static micromirrors are operated at few tens of hertz, well below their resonance frequencies. This mode of operation enables, for example, constant velocity scanning and static operation.

The following sections propose the design for a resonant translatory micromirror with vertical out-of-plane motion.

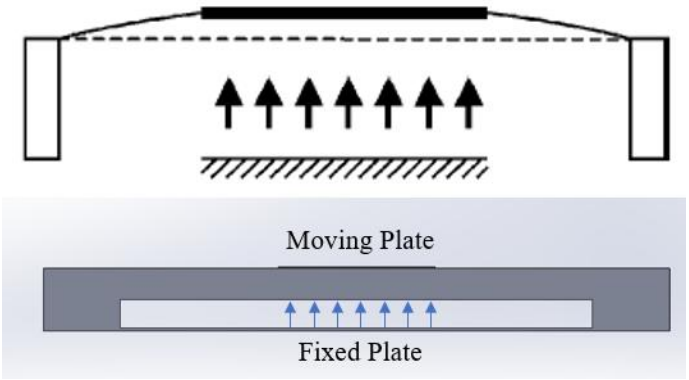

FIGURE 2: TRANSLATION MICROMIRROR DRIVEN BY A REPULSIVE-FORCE BASED ELECTROSTATIC ACTUATOR

DESIGN & WORKING PRINCIPLE

The flexure system is designed based on the FACT approach to design compliant mechanisms [9][10]. Since the desired DOF is a single translation DOF orthogonal to the reflective surface of the mirror, as per the FACT approach the constraints are chosen from the constraint space corresponding to 1 DOF Type 3, i.e., from parallel planes of constraints. The proposed design has a mirror with a reflective area of 1 mm^2 connected to ground by a parallel flexure system composed of two flexure blades in one plane and two flexure blades in another parallel plane. The flexure system is over-constrained by 7 to reduce parasitic error. The system is not under-constrained as there are no intermediate bodies between the ground and micromirror.

The topology was iteratively optimized to ensure all the other natural frequencies are at least an order of magnitude (x10) larger than the first natural frequency so that the mirror does not move with other unwanted DOFs.

Figure 1 shows the synthesized design of the micromirror. The design is intentionally kept simple for ease of fabrication. The design is also thermally stable. Dimensions for the design are limited by the fabrication capabilities available to the author. The dimensions of the flexure systems are as follows:

- Mirror aperture: 1 mm^2
- Mirror length: 1 mm
- Mirror width: 1 mm
- Mirror thickness: 0.2 mm
- Flexure blade(s) length: 1 mm
- Flexure blade(s) width: 1 mm
- Flexure blade(s) thickness: 10 μm

A [100] direction single crystal silicon is chosen as the candidate material for the flexure system. Silicon has outstanding mechanical properties and does not involve problems due to material stress. After removing the sacrificial layers below planar structures, they stay planar. A further huge advantage is the compatibility of silicon MEMS technology with the CMOS process which shall be discussed in detail in the following sections. Moreover, silicon has a very low coefficient of thermal expansion.

The micromirror uses a repulsive electrostatic force through parallel plate for actuation. The bottom surface of the mirror will

be the moving plate etched with electrodes and the substrate will be the fixed plate with electrodes. A repulsive force is induced between the fixed and moving capacitor plates. When a voltage is applied, the repulsive electrostatic force produced in the translation micromirror pushes the mirror plate up and away from its static position. The mirror plate moves back to its original position due to the restoring force from the supporting flexures. A repulsive-force based electrostatic actuation is chosen over attractive electrostatic actuation as there is no "pull-in" effect associated with this design and therefore the stroke is not limited by the initial space between the mirror plate and the substrate. Hence, the translating micromirror is able to modulate lights in a much wider spectrum. In addition, stiction does not happen in this design since the repulsive force pushes the mirror plate away from the substrate. Figure 2 shows the schematic of a repulsive-force electrostatic actuator that will be integrated in the design. Theoretically, the electrostatic force of surface electrostatic actuators can be formulated in the following equation:

$$F_{surface} = \varepsilon \cdot V^2 \cdot l_{surf} \cdot \frac{w_{surf}}{2} \cdot d^2$$

Where $F_{surface}$ is the electrostatic force due to the parallel plate actuator, V is the applied voltage, ε is permittivity of the media, l_{surf} and w_{surf} are the length and width of surface electrodes and d is the gap between the electrodes. The gap distance is crucial for the design.

MODAL ANALYSIS

The topology was iteratively optimized to minimize parasitic errors and achieve the desired mode shape separation. To calculate the mode shapes and the natural frequencies of the flexure system, first the twist-wrench mass matrix of the stage (in this case the micromirror) and the stiffness matrix of the flexure blades are generated for the synthesized topology using MATLAB. The modulus of elasticity of the chosen silicon material is 130 GPa and the modulus of rigidity is 50 GPa. The stiffness matrices for each of the flexure blade is calculated using Bernoulli-Euler beam bending equations. Since it is a parallel flexure system the stiffness of the four blades adds up as follows:

$$k_{TW} = k_1 + k_2 + k_3 + k_4$$

Where k_1, k_2, k_3, k_4 are the stiffness matrices of the four flexure blades. Figure 3 shows the effective twist-wrench stiffness matrix of the flexure system. Density of the chosen silicon is 2330 kg/m^3. Figure 4 shows the mass matrix of the micromirror. Figure 5 shows the six mode shapes of the micromirror and Figure 6 shows the corresponding natural frequencies in rad/sec. It can be seen that the second natural frequency of 1.0816 x 10^6 rad/sec is greater than the first natural frequency of 0.0334 x 10^6 rad/sec by more than an order of magnitude and all other natural frequencies are also larger by at least an order of magnitude.

The calculations from MATLAB are validated through FEA based modal analysis simulations in both ANSYS and SolidWorks. Figures 7 and 8 show the natural frequencies corresponding to the first and second mode shapes respectively from the FEA simulations of the modal analysis done in ANSYS. Figures 9 and 10 show the results from the modal analysis done in SolidWorks.

```
K_TW =

   1.0e+06 *

         0   -0.0005   -0.0078    5.2000         0         0
    0.0005         0    0.0078         0    5.2000         0
    0.0000   -0.0000         0         0         0    0.0005
    0.0000   -0.0000    0.0000         0    0.0005    0.0000
   -0.0000    0.0000    0.0000   -0.0005         0   -0.0000
    0.0000    0.0000    0.0000   -0.0078    0.0078         0
```

FIGURE 3: TWIST-WRENCH STIFFNESS MATRIX OF THE FLEXURE SYSTEM

```
M_TW =

   1.0e-06 *

         0   -0.0000   -0.0007    0.4660         0         0
    0.0000         0    0.0007         0    0.4660         0
    0.0007   -0.0007         0         0         0    0.4660
    0.0000   -0.0000    0.0000         0    0.0000    0.0007
   -0.0000    0.0000    0.0000   -0.0000         0   -0.0007
    0.0000    0.0000    0.0000   -0.0007    0.0007         0
```

FIGURE 4: MASS MATRIX OF THE MICROMIRROR

```
ModeShapes =

   -0.0000    0.0000   -0.7480    0.6021    0.0000   -0.0000
    0.0000    0.0000   -0.6638   -0.7984   -0.0000    0.0000
   -0.0000   -1.0000   -0.0000   -0.0000   -0.0000   -0.0000
   -0.0000   -0.0015   -0.0001   -0.0001    0.0000   -1.0000
    0.0000    0.0015    0.0001   -0.0001    1.0000   -0.0002
    1.0000    0.0000    0.0001   -0.0021    0.0000    0.0000
```

FIGURE 5: MODE SHAPES OF THE MICROMIRROR

```
Nat_freq =

   1.0e+06 *

    0.0334         0         0         0         0         0
         0    8.5166         0         0         0         0
         0         0    1.0816         0         0         0
         0         0         0    1.0816         0         0
         0         0         0         0    3.3405         0
         0         0         0         0         0    3.3405
```

FIGURE 6: NATURAL FREQUENCIES OF THE CORRESPONDING MODE SHAPES IN RAD/SEC

As can be seen the FEA results of the second natural frequency of 89,025 Hz is more than 10 times larger than the first natural

frequency of 7536.7 Hz i.e., by an order of magnitude larger and hence validates the results from MATLAB.

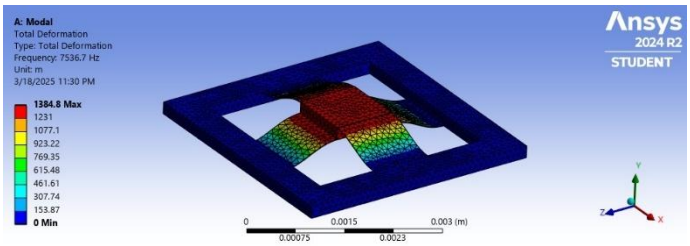

FIGURE 7: NATURAL FREQUENCY CORRESPONDING TO FIRST MODE SHAPE – FEA IN ANSYS

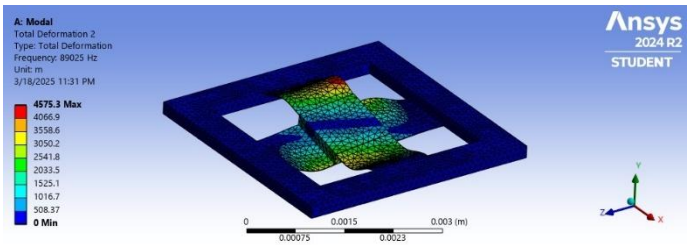

FIGURE 8: NATURAL FREQUENCY CORRESPONDING TO SECOND MODE SHAPE – FEA IN ANSYS

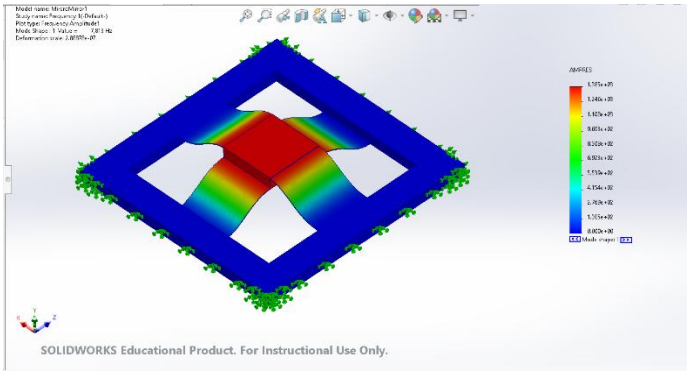

FIGURE 9: NATURAL FREQUENCY CORRESPONDING TO FIRST MODE SHAPE – FEA IN SOLIDWORKS

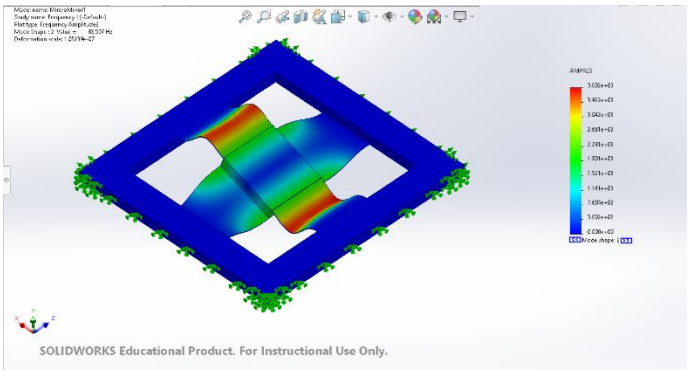

FIGURE 10: NATURAL FREQUENCY CORRESPONDING TO SECOND MODE SHAPE – FEA IN SOLIDWORKS

FABRICATION

The translatory micromirror can be manufactured in a CMOS compatible SOI process:

1. First a silicon-on-insulator (SOI) wafer is chosen with the device layer which defines the mirror and flexure blades, buried oxide (BOX) layer that acts as a sacrificial layer and handle layer which is the substrate that remains for electrode formation.
2. Wafer cleaning is done by removing organic, inorganic and particle contaminants using Piranha solution and HF dip.
3. The micromirror and flexure blades are patterned through photolithography. Photoresist is spin-coated onto the SOI device layer. It is exposed and micromirror, flexures and surrounding structures are developed using a mask aligner.
4. Etching is done using Deep Reactive Ion Etching (DRIE) on the device layer down to the BOX layer.
5. The buffered HF etch removes the BOX sacrificial layer, freeing the mirror and flexures. Supercritical CO_2 drying prevents stiction.
6. A thin metal layer of aluminium is deposited on the substrate and micromirror bottom surface. The parallel plate electrodes are defined through patterning using lift-off or wet etching. A thin aluminium layer is also deposited on the top surface to increase the reflectivity of the mirror.
7. Oxygen plasma cleaning is done to remove residual contaminants.

This fabrication process is ideal for the synthesized design due to high precision and aspect ratio control. DRIE etching allows precise fabrication of thin flexures and sharp geometries without over-etching. There is no need for multi-layer bonding, hence it will be a monolithic fabrication (single-wafer design). The buried oxide layer will ensure electrical isolation, making the parallel plate actuator implementation straightforward. Finally, CMOS compatibility allows integration with standard MEMS electronics if needed for sensing/feedback. Table 1 summarizes the time and cost estimates for each step of the fabrication process.

TABLE 1: TIME AND COST ESTIMATES OF THE FABRICATION PROCESS

Process Step	Time Taken	Cost Estimate
SOI Wafer Selection	Pre-fab process	$ 100-500 per wafer
Wafer Cleaning	30 min	Low ($5-10)
Photolithography	2-3 hours	Medium ($50-100)
DRIE etching	2-4 hours	High ($200-500
HF release etch	30 min – 1 hour	Medium ($50-100)
Metallization	1-2 hours	Medium ($100-300)
Final cleaning & packaging	1-2 hours	Variable ($50-200)

Therefore, the total time estimate for fabrication is ~8-12 hours per batch and the total cost estimate is ~$500-1500 per wafer (varies based on batch size and fab facility).

CONCLUSION

A simple flexure based resonant translating micromirror is designed using blade flexures in parallel planes while meeting the project requirements of having minimal parasitic error, avoiding under-constrained design and ensuring ease of fabrication. Future work can be done to develop an efficient design process by minimizing over-constrained design as well. The efficiency of other types of actuations including electromagnetic and electrothermal could be considered as future prospects.

REFERENCES

[1] Ahmad, M.; Bahri, M.; Sawan, M. "MEMS Micromirror actuation techniques: A comprehensive review of trends, innovation, and future prospects." Micromachines (2024) 15, 1233. DOI 10.3390/mi15101233.

[2] Caglar Ataman et al. "A fourier transform spectrometer using resonant vertical comb actuators." Journal of Micromechanics and Microengineering (2006): 16 2517. DOI 10.1088/0960-1317/16/12/001.

[3] Carminati, R., Costantini, S. "Micromirrors. In: Vigna, B., Ferrari, P., Villa, F.F., Lasalandra, E., Zerbini, S. (eds) Silicon Sensors and Actuators. Springer, Cham." (2022). DOI 10.1007/978-3-030-80135-9_18.

[4] Conant et al. "A flat high-frequency scanning micromirror."

[5] Drabe et al. "Accelerometer by means of a resonant micro actuator." MEMS/MOEMS Components and Their Applications Volume 5344 (2004). DOI 10.1117/12.524130

[6] F.-Y. Lee et al. "Design of a tunable resonant micromirror." Sensors and Actuators A 234 (2015) 72-81: DOI 10.1016/j.sna.2015.08.010

[7] He, Siyuan, and R. Ben Mrad. "Development of a novel translation micromirror for adaptive optics." Proc. SPIE 5264, Optomechatronic Systems IV, (2003): DOI 10.1117/12.515063.

[8] He, Siyuan, and R. Ben Mrad. "Large-stroke microelectrostatic actuators for vertical translation of micromirrors used in adaptive optics." IEEE Transactions on Industrial Electronics 52.4 (2005) 974-983: DOI 10.1109/TIE.2005.851682.

[9] J.B. Hopkins, M.L. Culpepper. " Synthesis of multi-degree of freedom, parallel flexure system concepts via Freedom and Constraint Topology (FACT)– Part I: Principles." Precision Engineering 34 (2010) 259-270: DOI 10.1016/j.precisioneng.2009.06.008

[10] J.B. Hopkins, M.L. Culpepper. " Synthesis of multi-degree of freedom, parallel flexure system concepts via freedom and constraint topology (FACT). Part II: Practice." Precision Engineering 34 (2010) 271-278: DOI 10.1016/j.precisioneng.2009.06.007

[11] J.B. Hopkins, M.L. Culpepper. " Synthesis of precision serial flexure systems using freedom and constraint topologies (FACT)." Precision Engineering 35 (2011) 638-649: DOI 10.1016/j.precisioneng.2011.04.006

[12] Liu et al. "State-of-the-Art Materials Used in MEMS Micromirror Arrays for Photonic Applications." Photonics (2024) 11, 253: DOI 10.3390/photonics11030253.

[13] Nakazawa, Kenta et al. "Resonant varifocal micromirror with piezoresistive focus sensor." Micromachines 7.4 (2016) 57: DOI 10.3390/mi7040057.

[14] Pengwang, E. et al. "Scanning Micromirror Platform Based on MEMS Technology for Medical Application." Micromachines (2016) 7, 24: DOI 10.3390/mi7020024

[15] R. Farrugia et al. "Design optimization of a high frequency resonating micro-mirror with low dynamic deformation." 2017 Symposium on Design, Test, Integration and Packaging of MEMS/MOEMS (DTIP), Bordeaus, France (2017): pp. 1-6. DOI 10.1109/DTIP.2017.7984467.

[16] Sandner et al. "Translatory MEMS actuators for optical path length modulation in miniaturized Fourier-transform infrared spectrometers." Journal of micro/nanlithography, MEMS and MOEMS 7.2 (2008) 021006-021006: DOI 10.1117/1.2945227

[17] Sandner et al. "Translatory MOEMS actuator and system integration for miniaturized Fourier transform spectrometers." Journal of Micro/Nanolithography, MEMS, and MOEMS 13(1), 011115 (2014): DOI 10.1117/1.JMM.13.1.011115

[18] Yuan Xue and Siyuan He. "A translation micromirror with large quasi-static displacement and high surface quality." Journal of Micromechanics and Microengineering 27 (2016) 015009: DOI 10.1088/0960-1317/27/1/015009.

[19] Yuan Xue et al. "A repulsive magnetic force driven translation micromirror" Journal of Micromechanics and Microengineering 27 (2017) 105008: DOI 10.1088/1361-6439/aa8779

[20] Yuan Xue. "Development of an electromagnetic actuator based translation micromirror as a movable mirror in a miniaturized FTIR spectrometer." (2018)

```
% This MATLAB script is written by Premkumar Sivakumar (UID: 506367127),
% to calculate the mode shapes and natural frequencies of the flexure system
% synthesized for the resonant translating micromirror

%%
% Assumed material properties
% for [100] direction single crystal silicon
E = 130 * 10^9; % Modulus of elasticity
G = 50 * 10^9; % Modulus of rigidity

Delta = [zeros(3,3) eye(3,3);
         eye(3,3) zeros(3,3)];

%% Flexure Body 1 (Blade flexure)

% Given dimensions
l1 = 1 * 10^-3; % length
b1 = 1 * 10^-3; % breadth
h1 = 0.01 * 10^-3; % height

% Location & unit vectors
L1 = [0.0015 0.001 -0.000005]';
n11 = [1 0 0]';
n12 = [0 0 -1]';
n13 = [0 1 0]';

% Transformation matrix
N1 = [n11 n12 n13 zeros(3,3);
      cross(L1,n11) cross(L1,n12) cross(L1,n13) n11 n12 n13];

% To compute polar moment of inertia, J2
sum = 0;
N = 1000;
for n = 1:2:N
    sum = sum + (1/n^5) * tanh(n*b1*pi/(2*h1));
end
J1 = ((h1^3 * b1) / 3) * (1 - (192 / pi^5) * (h1/b1) * sum);

% Moment of inertia, I
Ix1 = b1*h1^3/12;
Iy1 = h1*b1^3/12;
A1 = b1*h1;

% Temporary variables
u = l1/(E*Ix1);
v = -l1^2/(2*E*Ix1);
w = l1/(E*Iy1);
x = l1^2/(2*E*Iy1);
y = l1/(G*J1);
```

```
z = l1^3/(3*E*Iy1);
r = l1^3/(3*E*Ix1);
s = l1/(E*A1);

% Compliance matrix
C1 = [u 0 0 0 v 0;
      0 w 0 x 0 0;
      0 0 y 0 0 0;
      0 x 0 z 0 0;
      v 0 0 0 r 0;
      0 0 0 0 0 s];

% Stiffness matrix
S1 = C1^-1;

% Twist-Wrench Stiffness matrix
K1 = N1 * Delta * S1 * N1^-1;

%% Flexure Body 2 (Blade flexure)

% Given dimensions
l2 = 1 * 10^-3;
b2 = 1 * 10^-3;
h2 = 0.01 * 10^-3;

% Location & unit vectors
L2 = [0.001 0.0015 -0.000195]';
n21 = [0 -1 0]';
n22 = [0 0 -1]';
n23 = [1 0 0]';

% Transformation matrix
N2 = [n21 n22 n23 zeros(3,3);
      cross(L2,n21) cross(L2,n22) cross(L2,n23) n21 n22 n23];

% To compute polar moment of inertia, J2
sum = 0;
N = 1000;
for n = 1:2:N
    sum = sum + (1/n^5) * tanh(n*b2*pi/(2*h2));
end
J2 = ((h2^3 * b2) / 3) * (1 - (192 / pi^5) * (h2/b2) * sum);

% Moment of inertia, I
Ix2 = b2*h2^3/12;
Iy2 = h2*b2^3/12;
A2 = b2*h2;

% Temporary variables
```

```
u = l2/(E*Ix2);
v = -l2^2/(2*E*Ix2);
w = l2/(E*Iy2);
x = l2^2/(2*E*Iy2);
y = l2/(G*J2);
z = l2^3/(3*E*Iy2);
r = l2^3/(3*E*Ix2);
s = l2/(E*A2);

% Compliance matrix
C2 = [u 0 0 0 v 0;
      0 w 0 x 0 0;
      0 0 y 0 0 0;
      0 x 0 z 0 0;
      v 0 0 0 r 0;
      0 0 0 0 0 s];

% Stiffness matrix
S2 = C2^-1;

% Twist-Wrench Stiffness matrix
K2 = N2 * Delta * S2 * N2^-1;

%% Flexure Body 3 (Blade flexure)

% Given dimensions
l3 = 1 * 10^-3;
b3 = 1 * 10^-3;
h3 = 0.01 * 10^-3;

% Location & unit vectors
L3 = [0.0015 0.002 -0.000005]';
n31 = [-1 0 0]';
n32 = [0 0 -1]';
n33 = [0 -1 0]';

% Transformation matrix
N3 = [n31 n32 n33 zeros(3,3);
      cross(L3,n31) cross(L3,n32) cross(L3,n33) n31 n32 n33];

% To compute polar moment of inertia, J2
sum = 0;
N = 1000;
for n = 1:2:N
    sum = sum + (1/n^5) * tanh(n*b3*pi/(2*h3));
end
J3 = ((h3^3 * b3) / 3) * (1 - (192 / pi^5) * (h3/b3) * sum);

% Moment of inertia, I
```

```
Ix3 = b3*h3^3/12;
Iy3 = h3*b3^3/12;
A3 = b3*h3;

% Temporary variables
u = l3/(E*Ix3);
v = -l3^2/(2*E*Ix3);
w = l3/(E*Iy3);
x = l3^2/(2*E*Iy3);
y = l3/(G*J3);
z = l3^3/(3*E*Iy3);
r = l3^3/(3*E*Ix3);
s = l3/(E*A3);

% Compliance matrix
C3 = [u 0 0 0 v 0;
      0 w 0 x 0 0;
      0 0 y 0 0 0;
      0 x 0 z 0 0;
      v 0 0 0 r 0;
      0 0 0 0 0 s];

% Stiffness matrix
S3 = C3^-1;

% Twist-Wrench Stiffness matrix
K3 = N3 * Delta * S3 * N3^-1;

%% Flexure Body 4 (Blade flexure)

% Given dimensions
l4 = 1 * 10^-3;
b4 = 1 * 10^-3;
h4 = 0.01 * 10^-3;

% Location & unit vectors
L4 = [0.002 0.0015 -0.000195]';
n41 = [0 1 0]';
n42 = [0 0 -1]';
n43 = [-1 0 0]';

% Transformation matrix
N4 = [n41 n42 n43 zeros(3,3);
      cross(L4,n41) cross(L4,n42) cross(L4,n43) n41 n42 n43];

% To compute polar moment of inertia, J2
sum = 0;
N = 1000;
for n = 1:2:N
```

```
    sum = sum + (1/n^5) * tanh(n*b4*pi/(2*h4));
end
J4 = ((h4^3 * b4) / 3) * (1 - (192 / pi^5) * (h4/b4) * sum);

% Moment of inertia, I
Ix4 = b4*h4^3/12;
Iy4 = h4*b4^3/12;
A4 = b4*h4;

% Temporary variables
u = l4/(E*Ix4);
v = -l4^2/(2*E*Ix4);
w = l4/(E*Iy4);
x = l4^2/(2*E*Iy4);
y = l4/(G*J4);
z = l4^3/(3*E*Iy4);
r = l4^3/(3*E*Ix4);
s = l4/(E*A4);

% Compliance matrix
C4 = [u 0 0 0 v 0;
      0 w 0 x 0 0;
      0 0 y 0 0 0;
      0 x 0 z 0 0;
      v 0 0 0 r 0;
      0 0 0 0 0 s];

% Stiffness matrix
S4 = C4^-1;

% Twist-Wrench Stiffness matrix
K4 = N4 * Delta * S4 * N4^-1;

%% Stage 1

% Given material property
rho = 2330; % Silicon

% Given dimensions
l = 0.001;
b = 0.001;
h = 0.0002;
V = l*b*h;

% Location & unit vectors
Lm = [0.0015 0.0015 -0.0001]';
n1m = [1 0 0]';
n2m = [0 1 0]';
n3m = [0 0 1]';
```

```
% Transformation matrix
Nm = [n1m n2m n3m zeros(3,3);
      cross(Lm,n1m) cross(Lm,n2m) cross(Lm,n3m) n1m n2m n3m];

% Mass moments of inertia
Ixm = (rho*V)*(b^2 + h^2)/12;
Iym = (rho*V)*(l^2 + h^2)/12;
Izm = (rho*V)*(b^2 + l^2)/12;
inertia = [Ixm Iym Izm rho*V rho*V rho*V]';
In = diag(inertia);

%% Computing Mode Shapes and Natural Frequencies

K_TW = K1 + K2 + K3 + K4
M_TW = Nm * Delta * In * Nm^-1

[ModeShapes, EigenValues] = eig(inv(M_TW)*K_TW)

Nat_freq = sqrt(EigenValues)
```